

Wavelet-Based Methods for the Prognosis of Mechanical and Electrical Failures in Electric Motors

Wesley G. Zanardelli, Elias G. Strangas, Hassan K. Khalil

*Department of Electrical and Computer Engineering
Michigan State University
East Lansing, MI 48824, USA*

John M. Miller

*Ford Motor Co.
20901 Oakwood Blvd.
Dearborn, MI 48121, USA*

Abstract

The ability to give a prognosis for failure of a system is a valuable tool and can be applied to electric motors. In this paper, three wavelet-based methods have been developed that achieve this goal. Wavelet and filter bank theory, the nearest neighbor rule, and linear discriminant functions are reviewed. A framework for the development of a fault detection and classification algorithm based on the coefficients calculated from the discrete wavelet transform and using clustering is described. An experimental setup based on RT-Linux is described and results from testing are presented, verifying the analysis.

Key words: Fault Prognosis, Wavelets, DC Motors

1 Introduction

In recent years, industry has focused much attention on analytical methods to determine the state of health of systems. The state of health of a system can include information such as the existence and the type of imminent problems and an estimation of the remaining life expectancy. The ability to give a prognosis for the failure of a system is synonymous to detecting conditions that lead to reduced performance and eventual failure of the system. With this prognosis, attention can be brought to any problems a system may exhibit

before they cause the system to fail. The presence of small transient signals, superimposed on larger, perhaps noisy signals always present in the system, may indicate lack of health and a more or less imminent fault.

The electric motor is a prime example of a system, where failure occurring at an inopportune time can be inconvenient, expensive and dangerous. The current through an unhealthy electric motor is a non-stationary signal and the minor transients it may contain make Fourier methods unsuitable for analysis. Wavelets [1] on the other hand, are an excellent tool for the analysis of non-stationary signals. Using wavelet decomposition, information about the health of the system can be extracted from a signal over a wide band of frequencies and the analysis is localized in both the time and frequency domains.

In this work [2–4] the assumption was made that specific conditions leading to failures produce short transients on the currents of electrical motors. The analysis and computational tools to recognize these transients, or faults, were developed and applied to two types of automotive motors. For the remainder of this paper the term fault is defined as a condition of the motor that allows its continuous operation, but may eventually lead to failure. Detection of faults, combined with prior knowledge of their long-term effect on a motor, can be used to determine whether a prognosis for failure is appropriate. Motors selected for this study, with the exception of the healthy motors, all have faults thus defined, however none have failed.

Three techniques are used in this work to discriminate between machine faults. One technique is deterministic in nature and applies the results from the wavelet decomposition of the current through a machine to a decision tree [5] to identify and distinguish between faults. The second technique focuses on mapping the wavelet decomposition of the current into a multi-dimensional space, clustering the resultant vectors, and using several variants of the nearest neighbor rule [6] to distinguish faults. In the third technique, a set of trained weighting coefficients is applied to the wavelet decomposition of the current through a machine and the discriminant used as the criterion to distinguish between faults. Other techniques, such as neural networks, have been used for categorization of faults as well [7].

Signatures in the vibration of a machine are often used to detect mechanical faults. This requires the installation of an accelerometer, which can be bulky and adds additional cost. In [8], a three phase induction machine with a gear-box and its corresponding bearing assemblies are analyzed. In this case, only mechanical vibration is considered in the fault detection algorithm. The algorithm is able to detect the presence of a small ‘blip’ of 2mm diameter welded onto a gear tooth, a triangle shaped area missing from a gear tooth, and a fractured inner race of the bearing housing.

Three phase induction machines are analyzed for a stator open phase or a stator voltage unbalance in [9]. All three stator currents are measured and transformed to a two-phase representation. The Park's vector is analyzed using an Artificial Neural Network (ANN) to diagnose the machine for a stator voltage unbalance or an open phase. The occurrence of either of these faults manifests itself in the deformation of the current Park's vector pattern corresponding to a healthy condition. This deformation leads to an elliptic pattern whose major axis orientation is associated with the faulty phase. The severity of the deformation helps to distinguish between the two faults, with the open phase fault being the most deformed. A mathematical model of the induction motor is not required.

A model based fault detection scheme, using parameter estimation, is applied to brushless DC machines in [10]. The power inverter supply voltage, the DC current, and the mechanical angular velocity are measured. This is achieved by using the least-squares method to estimate R and k_E in the model for the electrical subsystem (1).

$$\bar{v}(t) = R\bar{i}(t) + k_E\omega_r(t) \quad (1)$$

The author uses the same technique to estimate J , c_c , and c_v in the model for the mechanical subsystem (2), where c_c is the Coulomb friction coefficient and c_v is the viscose friction coefficient. In the mechanical model, $k_T = k_E$.

$$J\dot{\omega}_r(t) = k_T\bar{i} - c_c\text{sign}(\omega_r(t)) - c_v\omega_r(t) \quad (2)$$

Through knowledge of these parameters, based on the electrical model, it can be determined if the phase resistance of all coils has increased, indicating an increase in stator temperature. It can also be determined if a broken coil exists. Based on the mechanical model, increases in Coulomb and viscose friction can be detected.

Permanent magnet brush DC machines are analyzed for the presence of an open phase / broken connector fault, shorting of adjacent commutator bars, and worn brush faults in [11]. In this work, DC current, DC voltage and mechanical angular velocity are measured. This model-based approach uses block-pulse function series techniques to estimate parameters in a continuous-time system. This is advantageous as it eliminates the need to discretize the system so that an algorithm like the least-squares method can be used. Also, it eliminates the need to transfer the discrete-time parameters back to continuous-time system parameters. The model parameters are converted to electromechanical parameters according to the relation given by the motor model. These parameters are passed to an ANN to determine the presence of the above mentioned faults.

A set of wavelets were introduced based on the shapes of widely encountered transient phenomena in the eddy currents on the surface of a steel mill in [12]. These new wavelets are high frequency oscillations enveloped by single and double-sided exponentials, a cosine-tapered rectangle, and Gaussian, Hanning and Hamming functions. A time-frequency scale distribution was developed and its power distribution was mapped onto a three dimensional image. Through analysis of these image patterns, detection and classification of faults is possible. Since the wavelets match specific transients, the modified wavelet transform can have a high sensitivity for certain applications.

In this paper, both mechanical and electrical faults are detected through the transients they cause in the armature current of the machine. This only requires the use of a current sensor, which is already in place in many drives. An accelerometer is not required. The detection and classification algorithms are implemented on brush DC windshield wiper and fuel pump motors.

In the windshield wiper motors, the following faults are investigated and the number of motors available with each fault is listed: One of the springs that normally keep the brushes in contact with the commutator face has become stuck due to excess sealant (3 motors); one of the springs that keep the brushes in contact with the commutator face has been kinked (3 motors); one gear tooth is removed from the gear reduction mechanism (3 motors); shaft misalignment because of a missing bushing (3 motors); insufficient grease applied to the speed reduction mechanism (5 motors); and the disk used by the motor to locate the correct parking position has been 'punched', causing the copper to be raised slightly. This results in the motor running through the park position for one or more revolutions (5 motors). In addition to the faulty motors, 3 healthy motors were available.

In the fuel pump motors, the following faults are investigated and the number of motors available with each fault is listed: One of the coils is poorly fused to the commutator causing its resistance to be increased (9 motors); one coil is cut entirely making its resistance infinite (7 motors); and the commutator face is scored (6 motors). In addition to the faulty motors, 6 healthy motors were available.

Although the faults present in the test machines were introduced intentionally during the assembly process, they represent conditions that can occur at any time during the life of the machine.

2 Background

2.1 Wavelets and Filter Banks

Classical frequency domain analysis, such as Fourier series, is best suited for stationary signals which are periodic in nature. The frequency content of a stationary signal does not change over time. Fourier series analysis provides the ability to localize a signal in frequency. Localization in time is not possible since the basis functions are sinusoids, which have an infinite amount of energy spreading out over all time. Since the faults in this work are not sinusoidal in nature, but rather short transients, a very large number of coefficients will be required of a Fourier representation.

Wavelets on the other hand, are a good tool for the analysis of non-stationary signals having transient behavior. The basis functions of a wavelet system, the scaling function $\varphi(t)$ and the wavelet function $\psi(t)$, have finite energy, which is concentrated around a point. This property gives a wavelet system the ability to localize any $L^2(\mathbf{R})$ signal in both time and frequency. The Hilbert space of measurable, square-integrable functions, $f(x) \in L^2(\mathbf{R})$, are the class of functions where (3) is true.

$$\int_{-\infty}^{+\infty} |f(x)|^2 dx < +\infty \quad (3)$$

Both scaling and wavelet functions can be derived from a single scaling or wavelet function by scaling and translation. A scaling function, $\varphi_{j,k}(t)$, both scales and translates a function $\varphi(t)$, where j is the \log_2 of the scale and $2^{-j}k$ represents the translation in time (4):

$$\varphi_{j,k}(t) = 2^{j/2} \varphi(2^j(t - 2^{-j}k)) \quad j, k \in \mathbf{Z} \quad \varphi \in L^2. \quad (4)$$

The same is true in the case of a wavelet function (5):

$$\psi_{j,k}(t) = 2^{j/2} \psi(2^j(t - 2^{-j}k)) \quad j, k \in \mathbf{Z} \quad \psi \in L^2. \quad (5)$$

The wavelet function $\psi(t)$ for the case where $j=k=0$ is often referred to as the mother wavelet.

A subspace of $L^2(\mathbf{R})$ is the scaling function space \mathcal{V} . $\varphi_{j,k}(t)$ spans the space \mathcal{V}_j , meaning that any function in \mathcal{V}_j can be represented by a linear combination of functions of the form $\varphi_{j,k}(t)$. The relationship between the span of scaling

functions with different indicies is shown in (6-7):

$$\cdots \subset \mathcal{V}_{-2} \subset \mathcal{V}_{-1} \subset \mathcal{V}_0 \subset \mathcal{V}_1 \subset \mathcal{V}_2 \subset \cdots \subset L^2 \quad (6)$$

$$\mathcal{V}_{-\infty} = \{0\}, \quad \mathcal{V}_{\infty} = L^2 \quad (7)$$

Another subspace of $L^2(\mathbf{R})$ is the wavelet vector space \mathcal{W} . A wavelet spans the space \mathcal{W}_j , which represents the difference between two scaling function spaces, \mathcal{V}_j and \mathcal{V}_{j+1} . The relationships in (8-9) show how the scaling and wavelet function spaces are nested.

$$\mathcal{V}_1 = \mathcal{V}_0 \oplus \mathcal{W}_0 \quad (8)$$

$$L^2 = \mathcal{V}_0 \oplus \mathcal{W}_0 \oplus \mathcal{W}_1 \oplus \cdots \quad (9)$$

Any function in $L^2(\mathbf{R})$ can be written as an expansion of a scaling function and wavelets (10), where $c_{j_0}(k)$ are the scaling function coefficients, $\varphi_{j_0,k}(t)$ is the scaling function at the initial scale j_0 , $d_j(k)$ are the wavelet function coefficients and $\psi_{j,k}(t)$ are the wavelet functions spanning the space between \mathcal{V}_{j_0} and L^2 .

$$f(t) = \sum_{k=-\infty}^{\infty} c_{j_0}(k) \varphi_{j_0,k}(t) + \sum_{k=-\infty}^{\infty} \sum_{j=j_0}^{\infty} d_j(k) \psi_{j,k}(t) \quad (10)$$

Wavelets have adaptive window size. This allows for good time resolution at low frequencies and good frequency resolution at high frequencies. The resulting time-frequency plane is shown in Fig. 1. This helps to identify transients containing both low and high frequencies.

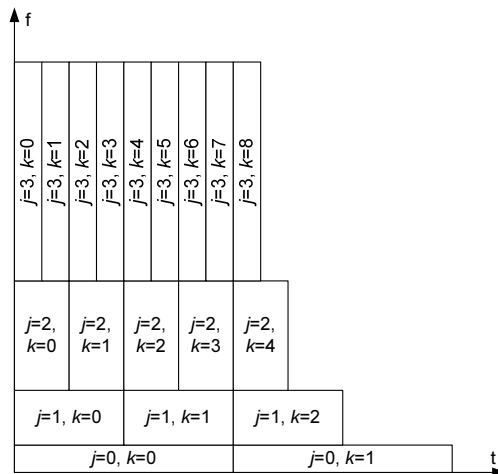


Fig. 1. DWT Time-Frequency Plane

The discrete wavelet transform is implemented on a computer using only additions and multiplications to perform convolutions. The scaling and wavelet function coefficients are calculated using filter banks. The scaling function coefficients are defined for a coarse scale from the scaling function coefficients at the next finer scale by convolving the coefficients at the finer scale with the recursion coefficients $h_0(n)$ and then down-sampling (11). $h_0(n)$ is often referred to as the decomposition low-pass filter. The same can be done in the case of the wavelet coefficients using the recursion coefficients $h_1(n)$ (12). $h_1(n)$ is often referred to as the decomposition high-pass filter.

$$c_j(k) = \sum_m h_0(m - 2k)c_{j+1}(m) \quad (11)$$

$$d_j(k) = \sum_m h_1(m - 2k)c_{j+1}(m) \quad (12)$$

2.2 Nearest Neighbor Rule

In order to categorize a sample point in d -dimensional space into a set of previously classified points, we use the nearest neighbor rule (1-NN). We assume that observations which are close to each other (in some appropriate metric) will have the same classification [13]. Using this technique, a method was developed based on wavelet analysis to recognize the presence of a fault and two different methods to discriminate between faults. We applied these techniques to two sets of DC automotive motors: windshield wiper motors and fuel pump motors. The current signals for the first were sampled during operation on wet and dry windshields at two different speeds, and for the second, operation at different fuel pressures.

2.3 Linear Discriminant Functions

A second approach to categorizing points in a d -dimensional space relies on the use of discriminant functions. In the implementation of discriminant functions, we assume no prior knowledge of a probability distribution among the sample points. The space is separated into K disjoint regions, each having its own weighting coefficients. In this work, we focus on the use of linear discriminant functions (13) [14],

$$D_k(\mathbf{x}) = x_1\alpha_{1k} + \dots + x_N\alpha_{Nk} + \alpha_{N+1,k} \quad k = 1, 2, \dots, K, \quad (13)$$

where x is the N -dimensional sample vector and α are the normalized weighting coefficients for the k -th class. A sample vector belongs to a particular class

if its discriminant function is greater for that class than for any other class, i.e., \mathbf{x}_i belongs to class C_j if

$$\boldsymbol{\alpha}_j^T \mathbf{x}_i > \boldsymbol{\alpha}_k^T \mathbf{x}_i \quad \text{for every } k \neq j.$$

The weighting coefficients are adjusted from their initial guess through a training procedure. The algorithm for this procedure makes adjustments to the weighting coefficients until each known sample vector is correctly classified. Young and Calvert [14] prove that this training algorithm will converge in a finite number of steps. When a known sample vector is correctly classified, no adjustment to the weighting coefficients is made. When one of the known sample vectors is incorrectly classified, or

$$\boldsymbol{\alpha}_j^T \mathbf{x}_i \leq \boldsymbol{\alpha}_l^T \mathbf{x}_i,$$

where

$$\boldsymbol{\alpha}_l^T \mathbf{x}_i = \max_{l \neq j} [\boldsymbol{\alpha}_1^T \mathbf{x}_i, \dots, \boldsymbol{\alpha}_K^T \mathbf{x}_i],$$

adjustments are made to $\boldsymbol{\alpha}_j$ (14) and $\boldsymbol{\alpha}_l$ (15) only,

$$\boldsymbol{\alpha}_j(i+1) = \boldsymbol{\alpha}_j(i) + a\mathbf{x}_i \tag{14}$$

$$\boldsymbol{\alpha}_l(i+1) = \boldsymbol{\alpha}_l(i) - a\mathbf{x}_i, \tag{15}$$

where a is a gain constant.

3 Analysis Methods

In building the detection and classification algorithm, fifteen mother wavelets were tried with the expectation that one or two would be used. Tables were built comparing the coefficients resulting from each mother wavelet over ten levels of decomposition.

This observation was used in the detection phase of the algorithm; it was considered that a fault is present when one of the wavelet transform modulus maxima exceeded this threshold of 5% above the maximum of the modulus maxima observed on new good motors. A lower threshold resulted in fault detection in healthy motors and a higher threshold increased the rate of non-detection of faults.

Results in Section 5 will show that for each fault there is a generally similar distribution of the coefficients exceeding the threshold values. This observation motivated the first approach, where a motor fault is categorized based on a decision tree.

The second method is based on the observations that:

- (1) The same fault may manifest itself on different motors with slight variations in the relative values of the coefficients that exceed the threshold corresponding to that fault,
- (2) the same fault, but of different degree of severity, will cause coefficients of neighboring levels to exceed the corresponding thresholds.

Here, the coefficients are mapped onto a d -dimensional sphere and categorized by distance.

The third method was developed in an effort to fine tune the previous minimum distance algorithm. It takes into account the fact that the clusters corresponding to each fault are not necessarily in the shape of d -dimensional spheres. It also introduces a way to train the weighting coefficients corresponding to each cluster.

Multiple wavelets were used in this work, and all performed relatively well. Depending on the type of transients present, however, different wavelets will outperform others. In general, wavelets which can represent the set of transients using fewer coefficients (sparse representation) will make the classification problem easier, plus the faults will be easier to visualize in the transform.

The objective of this work was not exact time localization of faults. The algorithms in this paper rely on the modulus maxima of the transform. The modulus maxima are the maximum of the absolute value of the coefficients at each scale, resulting in only 1 coefficient from each scale.

3.1 Classification Based on a Decision Tree

The first approach to the detection and classification problem was implemented on DC windshield wiper motors. The algorithm applies the modulus maxima of the wavelet coefficients from the first ten different levels of decomposition to a decision tree. Daubechies's D8 and the C18 Coiflet were used as mother wavelets for decomposition.

For the classification strategy, an additional localization parameter, α , is defined in (16) if and only if the criterion for detection is met, i.e. for at least one level of decomposition, i , the coefficient of the test motor, d_i was higher

than the threshold level \hat{d}_i , $d_i - \hat{d}_i > 0$.

$$\alpha = \frac{\sum_{i=1}^{10} (i \times (d_i - \hat{d}_i))}{\sum_{i=1}^{10} (d_i - \hat{d}_i)} \quad d_i - \hat{d}_i > 0 \quad (16)$$

Then the decomposition coefficients as well as the parameter α are used in a decision tree to categorize the fault.

3.2 Classification Based on the Unity Sphere Method

The second approach to the detection and classification problem was implemented on both windshield wiper and fuel pump motors and represents a refinement of the first. When examining the modulus maxima of the wavelet coefficients from the motors with the same fault as in the first method, it can be seen that the coefficients are not exactly the same, however they follow the same general pattern. In this analysis, these coefficients were represented as a ten-dimensional vector.

The classification part of the algorithm involves two steps: During the training part of the algorithm the lengths of the vectors from each motor with known faults are normalized, and the coefficients of the normalized vectors from faults of the same type are averaged. The resultant vectors serve as the centers of each fault cluster. The radius of each fault cluster is also determined in this stage, to include all the motors with a known fault.

In the characterization stage of a motor that has been determined to have a fault, again the vector corresponding to the coefficients resulting from wavelet analysis is normalized. Through this normalization only the direction of the coefficient vector determines the type of fault. The classification strategy consists then of finding the center of an already identified fault cluster, on the 10-dimensional unit sphere, which has the minimum Euclidean distance from the vector of the normalized coefficients of the test motor. If the normalized coefficient vector representing a test motor does not fall into one of the fault clusters, it is said that the motor does not have any of the known faults.

A two-dimensional example of this technique is shown in Fig. 2. Here an attempt is made to classify the point δ (which corresponds to a motor with fault A) as corresponding to either fault A or B, and therefore belonging to the corresponding cluster. Points marked with a circle belong to cluster A and points marked with squares belong to cluster B. The triangles represent the average of the vectors from each cluster. If δ is determined to belong to the cluster having the minimum Euclidean distance between δ and the cluster center, δ will be classified as part of cluster B rather than cluster A. This is

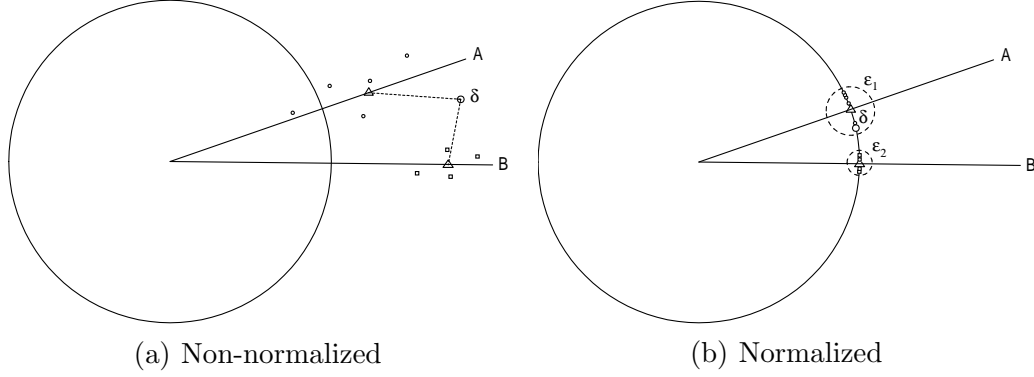


Fig. 2. Euclidean distance for a set of points

similar to how the motor faults manifest themselves in the ten-dimensional space. Experimentation showed that the motor faults could be classified much more accurately by using a normalized Euclidean distance, which is shown in Fig. 2(b). It is clear, after normalization that δ is closer to the center of cluster A.

If, however, δ were positioned slightly lower in the figure than it is, its normalized Euclidean distance would again classify it incorrectly as within B. This is due to the fact that cluster A has greater diameter than cluster B. To remedy this situation, a ball of radius ε was defined as a valid region for each cluster. This can be seen in Fig. 2(b) where ε_1 is the valid region for A and ε_2 is the valid region for B. Each test motor was therefore classified by finding its minimum normalized Euclidean distance within a radius ε from the center of each fault cluster. If the test motor did not fall within the radius ε_i from the center of any of the fault clusters i , it was classified as a good motor, or at least free of the faults which had been previously identified.

If the clusters on the unit sphere that correspond to each fault are small and distant from each other, then the algorithm discriminates accurately between faults. If, on the other hand, these clusters are large and the distance between their centers is small, then the algorithm is not as accurate. In the implementation of the second algorithm, the quality of the clustering was measured by the ratio of the average cluster radius to the average distance between clusters. An illustration of this is shown in Fig. 3, where A and B are clusters, x and z are their radii, and y is the distance between the centers of clusters A and B. All measurements are made on the unit circle. This discriminating ratio, r , in this case is defined as in (17):

$$r = 1 : \frac{y}{\frac{x+z}{2}}. \quad (17)$$

The only parameters required by the second algorithm were the modulus maxima of the coefficients from the decomposition, using the Biorthogonal 3.5

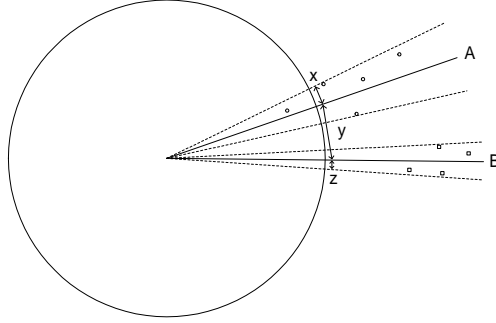


Fig. 3. Ratio of average cluster radius to average distance between clusters

mother wavelet. For the windshield wiper motors, data was only required from low speed dry windshield testing and for the fuel pump motors, data was only used from testing at 250 kPa. This was one-fourth the amount of data that was required for the first approach.

3.3 Classification Based on Discriminant Functions

The third approach to the classification problem was again implemented on both the windshield wiper and fuel pump motors. Instead of minimum distance, the maximum linear discriminant was used as a criterion.

The introduction of a training procedure made the classification algorithm more consistent. The initial guess for the weighting coefficients of each class was defined to be the mean of all of the known sample vectors in that class, i.e. in that particular fault. The initial weighting coefficients are identical to the averaged normalized vectors from faults of the same type from the classification step in the previous algorithm. These coefficients were then adjusted using the procedure described in Section 2.3 until all of the test motors with known faults were correctly classified. A gain constant of $a = 0.01$ was used to keep adjustments of the weighting coefficients small. The weighting coefficients from the mother wavelet that required the fewest number of corrections to converge were used in the algorithm. Through this training procedure, discriminant functions can produce more consistent results than the technique presented in Section 3.2.

The training procedure, however, could have undesirable effects if one of the motors specified as part of a particular class is considerably different than the others, possibly having multiple faults, or being an outlier in some other way. The weighting coefficients can adjust themselves so that each cluster is much larger than it would have been in the previous algorithm in order to accommodate all of its members.

4 Experimental Setup

4.1 Wiper Motor Experimental Setup

The experimental setup in the wiper motor testing is shown in Fig. 4. Torque profiles of the wiper system under different environmental conditions were applied. The torque profile for the wiper motor running in low speed mode on a dry windshield is shown in Fig. 5. The armature current passed through a hall

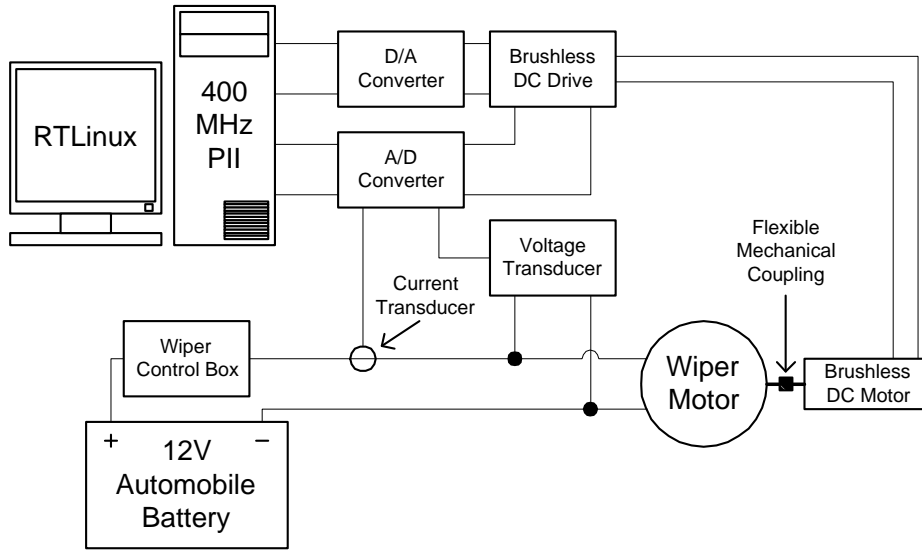


Fig. 4. Wiper motor experimental setup

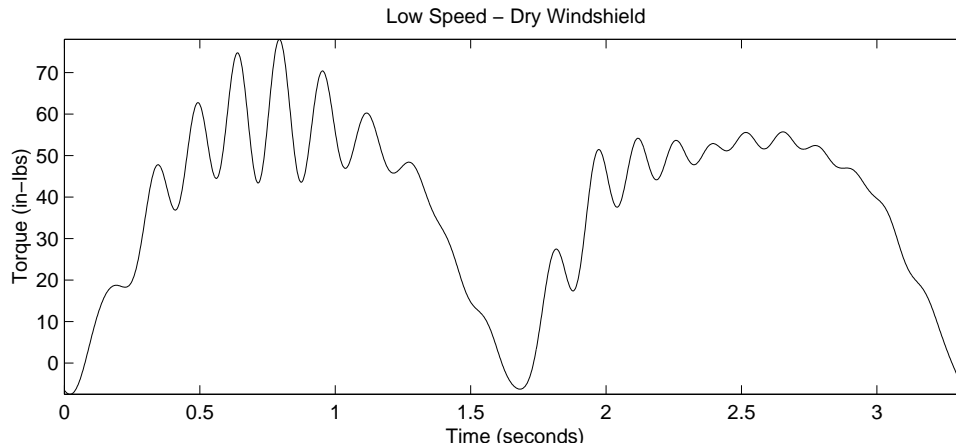


Fig. 5. Wiper motor profile for low speed operation on dry glass

effect transducer. The transducer output was sampled at 12.5kHz using a 12-bit A/D converter. To develop and test the various detection and classification algorithms, both new windshield wiper motors, as well as motors that were

manufactured to have specific faults known to significantly shorten their lives were analyzed.

4.2 Fuel Pump Experimental Setup

The experimental setup for the fuel pump motor testing is shown in Fig. 6. The armature current passed through a hall effect transducer. The transducer output was sampled at 16.7kHz using a 12-bit A/D converter. As with the wiper motors, both new fuel pump motors as well as motors that were manufactured to have specific faults known to significantly shorten their lives were analyzed.

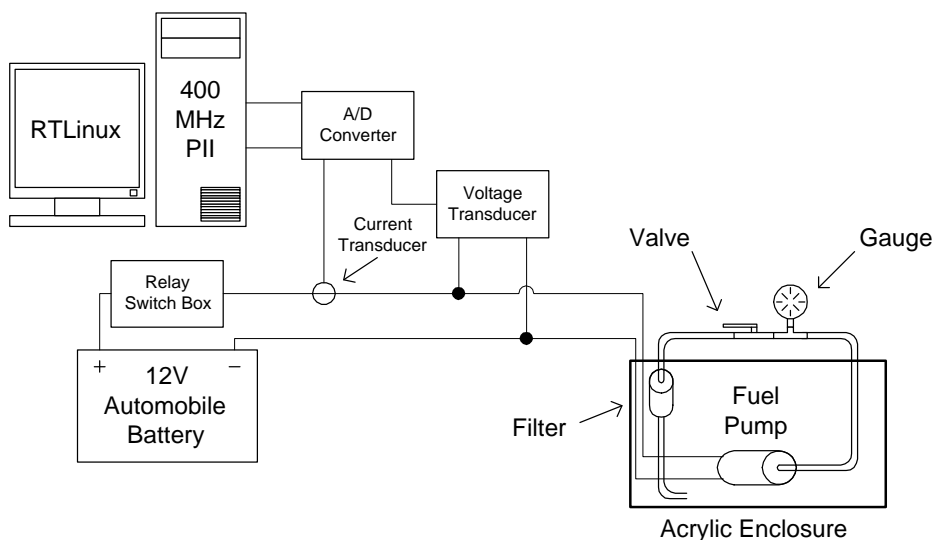


Fig. 6. Fuel pump experimental setup

5 Experimental Results

Experiments were conducted on a number of windshield wiper and fuel pump motors, both to determine the parameters needed and to categorize the motors. Tables 1, 2, and 3 give the wavelet coefficients at ten different scales, resulting from the analysis of the current in five motors, using a variety of mother wavelets, under the same operating conditions. The coefficients that exceeded the ones of ‘healthy’ motors by 5% are marked in black.

The raw data corresponding to Tables 2-3 are shown in Figs. 7-8 respectively. It can be observed in the case of the kinked spring that since higher frequency

Table 1
Modulus maxima of the wavelet coefficients for a motor with shaft misalignment (shaded coefficients are above the corresponding threshold)

Level	1	2	3	4	5	6	7	8	9	10
db1	0.717093	0.820063	0.752505	0.766853	0.900793	0.590006	0.879767	1.504751	4.140991	9.42641
db4	0.69268	0.707528		0.653901	0.946526	0.526287	0.541581	0.493274	0.758289	5.921158
db7	0.569517			0.749668	0.998592	0.475737	0.589265	0.513786	0.655265	4.898857
db10	0.630588	0.582064	0.607427	0.688686	1.007181	0.527558	0.528321	0.705984	0.514893	3.75176
bior2.2	0.513474		0.986833	0.899144	1.421163	0.717133	1.136949	0.986394	1.252359	5.20985
bior2.8	0.513474			0.862459	1.508311	0.509889	0.70256	0.749227	1.063549	5.566987
bior3.5	0.473636	1.033722		0.873671	2.025743	1.012536	1.141763	0.938268	1.20116	4.07039
bior6.8	0.55704			0.732841	1.06151	0.45079	0.580475	0.551084	0.647608	4.844287
coif1	0.605858		0.769876	0.71847	0.952749	0.560384	0.640424	0.709703	1.53381	7.227646
coif3	0.575787			0.725139	0.977852	0.446878	0.5685	0.508019	0.648964	5.39482
coif5	0.564062			0.736863	1.032048	0.435888	0.542352	0.480244	0.594193	
sym2	0.623361	0.800808	0.747439	0.724487	0.916117	0.547293	0.63882	0.756953	1.788106	6.331952
sym4	0.546735			0.679571	0.971832	0.575874	0.565442	0.48004	0.777677	5.795135
sym6	0.5443			0.733413	0.976857	0.511151	0.594311	0.50164	0.678997	5.235544
sym8	0.544479			0.731826	0.961435	0.445064	0.571001	0.492958	0.631554	5.053121

Level	1	2	3	4	5	6	7	8	9	10
db1		0.826322	0.730372	0.691732	0.798983	0.456981	0.872021	1.587696	4.165889	10.02897
db4		0.788259		0.591608	0.851694	0.350834	0.429406	0.442357	0.904319	5.300098
db7				0.628284	0.898655	0.31251	0.453662	0.402881	0.746629	5.274361
db10		0.622199	0.587454	0.630435	0.910626	0.290563	0.41254	0.413045	0.66748	4.759
bior2.2	0.63299	0.834147	0.987662	0.819769	1.316728	0.560204	0.897954	0.85479	1.193269	5.900039
bior2.8	0.63299		0.93891	0.729246	1.462225	0.359576	0.514715	0.670696	1.213433	6.107591
bior3.5		0.834147	1.146244	0.760775	1.949106	0.609384	1.065876	0.964778	1.067884	2.854382
bior6.8	0.697716			0.5786	1.068783	0.287251	0.432271	0.446129	0.519302	4.79501
coif1	0.733523		0.795793	0.668446	0.890702	0.412417	0.481984	0.620405	1.756283	7.518838
coif3	0.719335		0.716835	0.595324	0.988765	0.32513	0.425861	0.424504	0.529224	5.277242
coif5	0.711795			0.613053	0.937002	0.264622	0.394169	0.413949	0.603606	3.721771
sym2	0.769987	0.852382		0.653797	0.894325	0.339856	0.469755	0.535556	1.627138	7.73751
sym4		0.852382	0.722007	0.583315	0.93874	0.438712	0.458667	0.473155	0.663723	5.862317
sym6		0.852382		0.576578	0.946864	0.374795	0.423302	0.416146	0.528854	5.056883
sym8		0.852382	0.721757	0.579698	0.985539	0.289957	0.411865	0.413753	0.546052	4.895758

Level	1	2	3	4	5	6	7	8	9	10
db1	0.79677			0.873271	1.060147	0.622872	1.155317	1.550137	4.215688	9.854437
db4		0.749646	0.690037	0.811524	1.116601	0.490156	0.631988	0.656383	0.906199	5.628133
db7	0.656364	0.658203	0.618599	0.754815	1.150876	0.460059	0.490921	0.567373	1.103164	4.392732
db10		0.590935	0.559203	0.878686	1.120792	0.366046	0.513157	0.535771	0.615391	3.400422
bior2.2	0.610857		1.01353	1.049923	1.45229	0.913676	1.490278	0.992435	1.788413	5.671198
bior2.8	0.610857		0.968872	1.00073	1.596031	0.604099	0.655149	0.883687	1.422175	5.621316
bior3.5	0.542246	1.021978	1.176774	1.133381	2.34987	1.068038	1.433092	1.093838	1.073193	3.877563
bior6.8	0.654908	0.770512		0.793075	1.209837	0.447794	0.522811	0.605361	0.725346	3.701112
coif1	0.729718	0.830472		0.856566	1.015279	0.585558	0.681679	0.684572	1.861496	7.722182
coif3	0.681149	0.802248	0.754393	0.794596	1.126368	0.465887	0.528102	0.576031	0.712375	4.021609
coif5	0.665032	0.752282		0.725734	1.102482	0.41286	0.506336	0.536795	0.754062	3.121422
sym2	0.76628	0.791867		0.775866	1.076362	0.558434	0.645622	0.770003	2.162294	7.643172
sym4	0.658727	0.756272		0.786391	1.062282	0.478361	0.527436	0.57286	1.057089	5.384972
sym6	0.652568	0.754969		0.794017	1.080811	0.474069	0.534605	0.575611	0.762755	4.087421
sym8	0.64971	0.754969	0.720263	0.795805	1.134761	0.44812	0.515822	0.5589	0.690876	3.511588

Table 2
Modulus maxima of the wavelet coefficients for a motor with a kinked spring (shaded coefficients are above the corresponding threshold)

Level	1	2	3	4	5	6	7	8	9	10
db1	0.513474	0.582182	0.756932	1.145583	1.739614	1.508664	2.496546	3.807655	5.29666	9.715154
db4	0.422865	0.429809	0.603463	0.950324	2.300884	0.99721	1.214328	3.483603	1.241646	4.060825
db7	0.41593	0.394768	0.58911	1.0034	1.828488	0.890732	1.878576	3.363273	2.410558	4.484548
db10	0.369776	0.30445	0.461134	0.965922	1.98793	0.755256	1.649983	3.521698	2.382792	4.490138
bior2.2	0.393959	0.522712	0.913104	1.346343	2.437904	1.596848	2.363289	3.697593	5.597795	4.943661
bior2.8	0.393959	0.470764	0.825215	1.534214	2.536372	1.501542	2.234632	3.693707	4.861101	5.541678
bior3.5	0.336414	0.502464	1.095436	1.322298	3.437006	1.534607	2.884319	5.287654	8.946649	3.531382
bior6.8	0.42635	0.434695	0.606614	1.151994	1.338229	1.138126	1.740938	3.115566	2.96733	4.506663
coif1	0.472075	0.467598	0.732248	1.320279	1.93439	1.228725	2.568532	4.273147	3.87351	6.596554
coif3	0.444789	0.426173	0.544751	1.130599	1.302333	1.140047	1.947739	3.07169	2.594194	4.932113
coif5	0.437515	0.409235	0.69339	1.006335	1.812672	1.005935	1.837904	3.175818	2.381632	4.221958
sym2	0.443115	0.491402	0.73251	1.242516	1.764953	1.241268	2.305211	3.70207	1.830773	7.995317
sym4	0.443502	0.477825	0.73251	1.209618	1.910022	1.151371	2.403285	3.354932	2.930309	4.601186
sym6	0.43862	0.427136	0.617977	1.32771	1.886686	1.184823	2.107537	3.451377	2.77247	4.654624
sym8	0.435855	0.41157	0.614932	1.145949	1.898883	1.094035	1.803282	3.481211	2.562228	4.530842

information is present in the waveform, coefficients in the lower scales of the DWT exceed their corresponding thresholds.

Of the windshield wiper motors the first algorithm was able to detect and classify correctly 16 of the 19 motors used. The second algorithm was able to detect the presence or absence of faults in 23 of the 24 motors tested, and to correctly classify 20 of 21 motors with faults. Of the fuel pump motors, the second algorithm was able to detect the presence or absence of faults in 27 of the 28 motors tested, and to correctly classify 21 of 22 motors with faults. The third algorithm had the same criterion for detection as the second algorithm,

Table 3

Modulus maxima of the wavelet coefficients for a motor with insufficient gear grease (shaded coefficients are above the corresponding threshold)

Level	1	2	3	4	5	6	7	8	9	10
db1	0.646269	0.663561	0.588724	0.791892	1.000389	0.835733	1.279259	2.953945	5.498597	5.560228
db4	0.561365	0.573707	0.505324	0.729722	1.090303	0.839333	0.712122	0.854309	1.321452	1.413436
db7	0.514442	0.491153	0.453078	0.689727	1.207884	0.342286	0.812168	0.804804	1.261869	0.978865
db10	0.541019	0.447667	0.435444	0.796316	1.203778	0.446171	0.57411	0.780158	1.010741	0.938865
bior2.2	0.482488	0.652607	0.739779	0.817128	1.523296	0.834381	1.411862	1.384348	2.180015	1.428266
bior2.8	0.482488	0.618056	0.715968	0.857362	1.756006	0.627119	0.973147	1.597413	2.320773	1.016416
bior3.5	0.451503	0.697576	0.834557	1.169104	2.305631	0.895044	1.740163	1.667718	1.541356	0.976839
bior6.8	0.534394	0.546305	0.559736	0.73252	1.270019	0.521261	0.788228	0.908929	0.932877	0.444127
coif1	0.566576	0.580389	0.574688	0.753122	1.115104	0.511131	0.845	1.349346	3.249909	1.920615
coif3	0.549131	0.549624	0.480131	0.745358	1.206512	0.456169	0.790675	0.809716	1.077559	0.227276
coif5	0.545279	0.534005	0.520833	0.810629	1.18016	0.464684	0.803008	0.826633	0.837175	0.223895
sym2	0.610369	0.666562	0.538594	0.747102	1.060233	0.556836	0.822889	1.153094	2.928657	1.921282
sym4	0.549269	0.61526	0.477629	0.731368	1.128973	0.367594	0.70255	0.880617	1.776192	1.117833
sym6	0.541391	0.557133	0.494215	0.770879	1.144058	0.441942	0.751476	0.819115	1.198038	1.15546
sym8	0.535454	0.563422	0.519535	0.748373	1.229421	0.465468	0.780527	0.80036	0.938683	1.105533

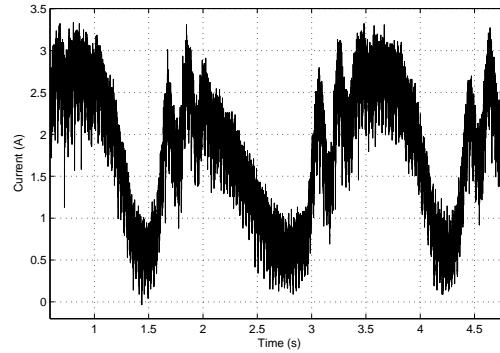


Fig. 7. Kinked Spring - Low Speed, Wet Windshield

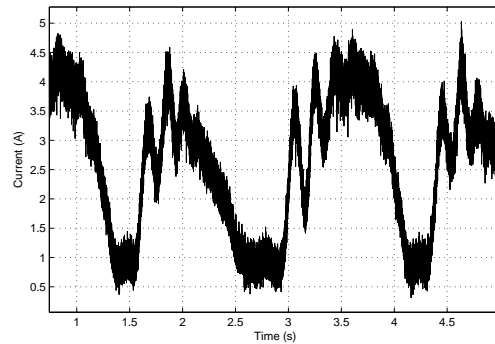


Fig. 8. Insufficient Gear Grease - Low Speed, Wet Windshield

thereby producing the same results. It was able to correctly classify 21 of 21 windshield wiper motors with faults and 22 of 22 fuel pump motors with faults.

In the implementation of the first algorithm, it was observed that the modulus maxima of the coefficients of the wavelet transform for all of the motors having a given type of fault manifest themselves in a unique way. It was also observed that the localization parameter remained relatively constant for all motors with the same fault type. Motors having other faults showed similar behavior in that the modulus maxima of their wavelet coefficients manifested themselves in a similar way to each other but differently from motors with other faults.

Results from the second algorithm show that for the wiper motor analysis, the discrimination ratio was 1 : 3.876, and for the fuel pump motor analysis the

ratio was 1 : 0.890. In any case, a higher ratio indicates more closely spaced points and better separation between clusters.

In the implementation of the third algorithm, further testing is being done to show that it is possible to achieve the same quality of results demonstrated here while only using a subset of the available motors to train the weighting coefficients.

6 Conclusions

Three techniques have been developed and were used to detect and classify conditions in electric motors, defined as faults, that will result in a reduction in performance and eventual failure. The approaches developed would be useful in several situations, in particular as a system to monitor the health of electric motors either in a vehicle or at the end of an assembly line. By using these strategies, a prognosis for the failure of an electric motor can be made. Although all three algorithms performed well, the second showed the best balance between ease of implementation and accuracy, as it could adapt to different types of faults, and few subjective decisions regarding its implementation were required. Measures of quality of performance were developed for the second method. The third algorithm shows much promise, however further testing is required.

All three methods were implemented in the laboratory and experiments validated them.

References

- [1] C. S. Burrus, R. A. Gopinath, H. Guo, Introduction to Wavelets and Wavelet Transforms, A Primer, Prentice Hall, 1998.
- [2] W. G. Zanardelli, E. G. Strangas, H. K. Khalil, J. M. Miller, Comparison of Wavelet-Based Methods for the Prognosis of Failures in Electric Motors, IEEE Workshop on Power Electronics in Transportation (2002) 61–67.
- [3] W. G. Zanardelli, E. G. Strangas, H. K. Khalil, J. M. Miller, The Use of Wavelet Analysis and the Nearest Neighbor Rule for the Prognosis of Failures in Electric Motors, IEEE International Symposium on Diagnostics for Electrical Machines, Power Electronics and Drives (2001) 591–596.
- [4] W. G. Zanardelli, The Use of Wavelet Analysis for the Prognosis of Failures in Electric Motors, Master’s thesis, Michigan State University (2000).

- [5] A. R. Webb, *Statistical Pattern Recognition*, 2nd Edition, John Wiley & Sons, 2002.
- [6] J. H. Friedman, F. Baskett, L. J. Shustek, An Algorithm for Finding Nearest Neighbors, *IEEE Transactions on Computers* C-24 (10) (1975) 1000–1006.
- [7] D. Chen, W. J. Wang, Classification of Wavelet Map Patterns Using Multi-Layer Neural Networks for Gear Fault Detection, *Mechanical Systems and Signal Processing* 16 (4) (2002) 695–704.
- [8] B. A. Paya, I. I. Esat, M. N. M. Badi, Artificial Neural Network Based Fault Diagnostics of Rotating Machinery Using Wavelet Transforms as a Preprocessor, *Mechanical Systems and Signal Processing* 11 (1997) 751–765.
- [9] H. Nejari, M. E. Benbouzid, Monitoring and Diagnosis of Induction Motors Electrical Faults Using a Current Park's Vector Pattern Learning Approach, *IEEE Transactions on Industry Applications* 36 (2000) 730–735.
- [10] O. Moseler, R. Isermann, Application of Model-Based Fault Detection to a Brushless DC Motor, *IEEE Transactions on Industrial Electronics* 47 (2000) 1015–1020.
- [11] X. Q. Liu, H. Y. Zhang, J. Liu, J. Yang, Fault Detection and Diagnosis of Permanent-Magnet DC Motor Based on Parameter Estimation and Neural Network, *IEEE Transactions on Industrial Electronics* 47 (2000) 1021–1030.
- [12] W. J. Wang, Wavelets for Detecting Mechanical Faults with High Sensitivity, *Mechanical Systems and Signal Processing* 15 (4) (2001) 685–696.
- [13] T. M. Cover, P. E. Hart, Nearest Neighbor Pattern Classification, *IEEE Transactions on Information Theory* IT-13 (1) (1967) 21–27.
- [14] T. Y. Young, T. W. Calvert, *Classification, Estimation and Pattern Recognition*, American Elsevier Publishing Co., Inc., 1974.